Journal of Applied Polymer Science

Inherently Adaptive Polymer Nanocomposites

Mohammad Sayayr,[1] Rankothge R. Weerasiri,[2] Anagi M. Balachandra,[2] Parviz Soroushian[1]
[1]Department of Civil Engineering and Environmental Engineering, Michigan State University, East Lansing, Michigan
[2]Technova Corporation, 1926, Turner Street, Lansing, Michigan
Correspondence to: A. M. Balachandra (E-mail: anagi@technovacorp.com)

ABSTRACT: A new class of inherently adaptive polymer nanocomposites is developed where stress-enabled redox reactions are used in the context of a solid polymer electrolyte to form deposits which render mechanical strengthening effects. Experimental investigations were conducted to provide insight into this self-adaptation phenomenon. Results of tests conducted on bolted composite joints demonstrated the occurrence of this self-adaptation phenomenon. Experiments were also performed on cracked composite specimens where the potential of the self-adaptation phenomenon to repair cracks was demonstrated. © 2014 Wiley Periodicals, Inc. J. Appl. Polym. Sci. **2014**, *131*, 40620.

KEYWORDS: composites; mechanical properties; redox reactions; solid polymer electrolyte

Received 25 October 2013; accepted 18 February 2014
DOI: 10.1002/app.40620

INTRODUCTION

Self-adaptation and self-healing capabilities can substantially enhance the safety and reliability of structural systems.[1,2] Inherently adaptive materials are defined here as materials with an intrinsic capability to mobilize their resources or modify their structure in response to local stress rise and damaging phenomena to locally reinforce the critical area and mitigate failure.[1,3–6] Self-adaptation features can prevent catastrophic growth of critical defects which evolve in structural materials during manufacturing and in service.[7]

The self-adaptation capabilities of biological materials such as bone[8–10] provide the inspiration for development of synthetic materials with inherently adaptive capabilities.[11,12] Bone uses a powerful control mechanism to reconfigure its structure to remove stress gradients generated after damaging effects for optimum performance. This self-adaptation phenomenon is guided by the electrical potential gradient generated in bone under stress gradient which drives the transport of bone substance toward areas experiencing higher levels of compressive stress. The transport process eliminates stress gradient, and promotes an optimum structural performance with structural substance concentrated along compressive stress paths.[13]

Previous studies on development of synthetic self-healing and adaptive materials and components can be broadly categorized into three groups. One concept proposed for development of self-healing polymer matrix composites incorporates a microencapsulated healing agent and a solid chemical catalyst within the polymer matrix.[14,15] Healing is triggered by crack propagation through the microcapsules, which then release the healing agent into the crack plane. Subsequent exposure of the healing agent to the chemical catalyst initiates polymerization to bond the crack surfaces.

Some other self-healing materials use ionomers,[2,16] which are a class of ion-containing copolymers with maximum ion group content of ~15 mol%.[17,18] Their bulk properties are governed by ionic interactions within discrete regions of the polymer structure. Gains approaching (or exceeding) 100% in tensile strength, toughness, and elastic modulus can be realized with moderate to high ionic contents when compared with polymers with no ionic content.[19] The order–disorder transition of ionomers upon heating and cooling provides them with the ability to heal punctures made through them by projectile impact.[20] It is hypothesized that healing occurs if sufficient energy is transferred to the polymer under impact to heat the material above the order–disorder transition where disordering of the polymer aggregation occurs. Following puncture, removal of this heat energy leads to reordering of the ionic aggregations and thus healing of the ionomer.

Some emerging self-adapting materials use mechanical stress to trigger chemical reactions.[21] This approach seeks to develop the ability to efficiently and selectively overcome all thermodynamic reaction barriers, so that any reactant can be converted to a desired product.[22] Traditionally, chemists use catalysts, heat, light, and sometimes electric fields to break down these barriers. More recently, nature's enzyme-accelerated reactions, either by building enzyme-like nanoscale reaction vessels[23] or via self-aggregation of reactants,[24] are used to modulate reactivity.

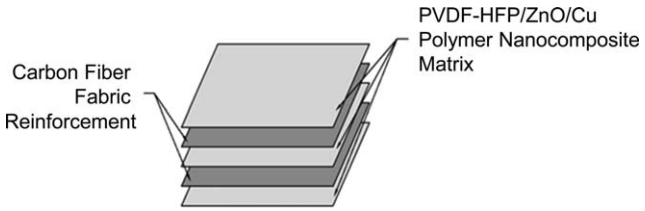

Figure 1. Preparation of the polymer laminated nanocomposites/carbon fiber laminates.

Whether self-healing and adaptive phenomena occur via nonautonomous (requiring an external trigger like heat or light) or autonomous (not requiring any external trigger; the damage itself is the stimulus for the healing), the phenomenon benefits structural reliability and longevity, and reduces maintenance/repair costs. Most previous concepts proposed for development of adaptive and self-healing materials incorporate extraneous constituents (e.g., microcapsules or nanocapsules), which are not integral constituents of the structural material in the system.[14,21,25,26] In some cases where intrinsic self-healing phenomena do occur, heating (>100°C) is required to prompt such phenomena.[27,28] This investigation presents an approach to self-adaptation where stress-induced electrochemical oxidation–reduction reactions are used in the context of a solid electrolyte with metal ions which are reactively incorporated into the solid polymer electrolyte, yielding an inherently adaptive polymer nanocomposite. The self-adaptation and self-healing mechanisms and implications of this system were validated experimentally in application to bolted joints and cracked composites, respectively.

MATERIALS AND METHODS

Materials

Poly(vinylidine fluoride-*co*-hexafluropropylene) (PVDF-HFP) pellets with 15% hexafluropropylene (HFP) and average molecular weight, M_w, of ~400,000, copper(II) trifluoromethane sulfonate (CuTf), ethylene carbonate (EC), propylene carbonate (PC), tetrathydrofuran (THF), and zinc oxide (ZnO) nanoparticles with average particle size of ~30 nm, and copper nanoparticles with average particle size of ~80 nm were purchased from Sigma-Aldrich. ZnO nanoparticles were subjected to 300°C heat treatment in air for 10 min, and then to 500°C for 1 h; they were allowed to cool down to room temperature. All other materials were used as purchased.

Preparation of Polymer Electrolyte

Three gram (18% by weight) of PVDF-HFP was dissolved in 55 mL of THF at 60°C while stirring. Subsequently, CuTf (1.8 g), EC (3.5 g), and PC (1.8 g) were added to the mixture (70 wt % total, with CuTf : EC : PC ratio of 1.0 : 8.0 : 3.5), and stirred until a uniform solution was obtained. The final solution was cast into a container, and left overnight for solvent evaporation at room temperature.

Preparation of Polymer Nanocomposite

The PVDF-HFP solid electrolyte was prepared as described earlier. Subsequently, heat-treated ZnO and copper nanoparticles were dispersed separately in THF, sonicated, and then repeatedly subjected to sonication in an ice bath and then centrifuged for thorough dispersion of ZnO and copper nanoparticles. The supernatants were added to the PVDF-HFP mixture, and the resulting blend was subjected to repeated sonication and centrifuging to achieve a uniformly dispersed blend. Just before casting, the blend was sonicated for a final time.

Preparation of Polymer Nanocomposite/Carbon Fiber Laminates

A carbon fiber fabric was cut into the required size and was exposed to UV/ozone for 30 min on each side. To complete the functionalization process, carbon fabrics were immersed in concentrated hydrochloric acid solution for 3 days. The resulting functionalized carbon fabric was rinsed with copious amounts of deionized water and allowed to dry. Finally, the fabric was cleaned in UV/ozone for 30 min on each side to remove any acid residues.

A laminated composite of PVDF-HFP/ZnO/Cu polymer nanocomposite matrix and carbon fiber fabric reinforcement was prepared by alternately placing the polymer nanocomposite and the coated woven carbon fabric inside a mold as shown in Figure 1.

The carbon fiber fabric volume fraction in the composite was 17%. Solvent evaporation over time led to the formation of a laminated carbon fiber polymer nanocomposite where the polymer nanocomposite matrix was bonded to the functionalized carbon fiber reinforcement.

Bolted composite joints (Figure 2) were prepared with the laminated composite sheets joined using steel bolts, nuts, and washers.[29] The dimensions of the bolted composite joint are presented in Figure 2. This single-lap shear test specimen is anticipated to exhibit the shear-out mode of failure.

The joint specimen was subjected to a sustained tensile load that was 50% of its peak load using the experimental setup shown in Figure 3. The electric potential difference and electric current flowing between the critically stressed area near the bolt and the normally stressed area midway between the bolt and the end grip were monitored over time under sustained loading. The electrical potential measurements were carried out with Agilent Technologies DSO1024A digital oscilloscope and Keithley precision digital multimeter capable of measuring voltages in the range of 1 μV to 20 V on one range with a sensitivity of

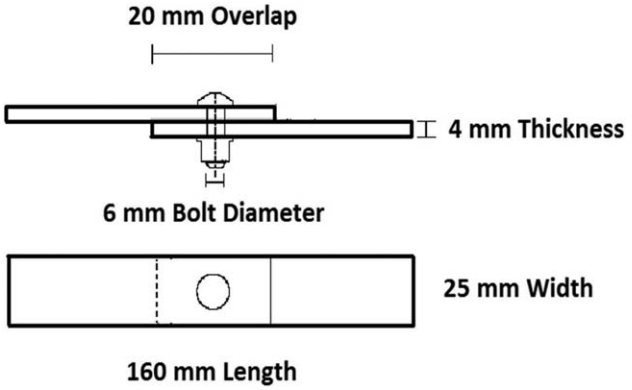

Figure 2. Configuration of the bolted specimen.

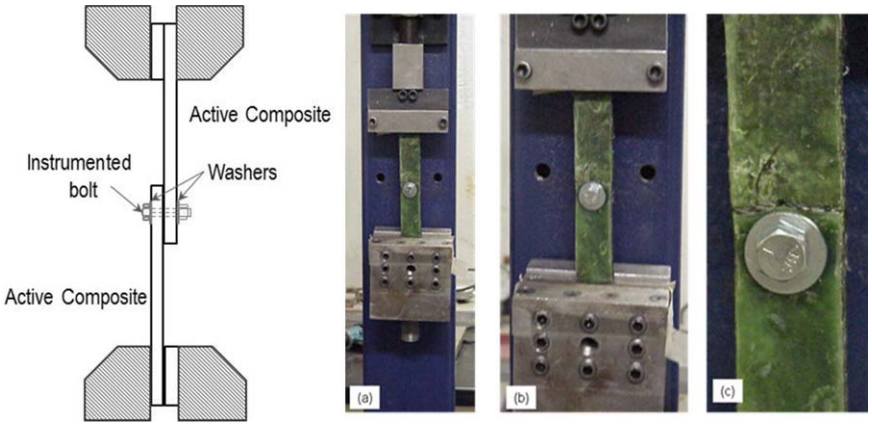

Figure 3. Bolted joint test setup. [Color figure can be viewed in the online issue, which is available at wileyonlinelibrary.com.]

1% in a selected range. After application of the sustained load over 2 weeks, the specimen was tested to failure in tension. Tension tests were carried out with a MTS load frame equipped with MTS 406 Servo Controller, load cell, LVDT, and data acquisition system.

RESULTS

A bolted joint between composite sheets with the solid polymer electrolyte nanocomposite matrix was subjected to sustained loading. The sharp stress gradient at the interfaces within the joint area would guide and drive deposition phenomena which enhance the mechanical performance of the joint. Measurement of voltage between the highly stressed region near the bolt and the normally stressed region midway between the bolt and the end grip [Figure 4(a)] confirmed that an electric potential gradient developed within the solid polymer electrolyte nanocomposite. The electric potential difference recorded over 14 days under sustained loading is presented in Figure 4(b). Ten measurements were made daily, and Figure 4(b) presents the mean values and ranges of daily measurements. The electrical potential measurements were carried out with an Agilent Technologies DSO1024A digital oscilloscope, for each potential measurement this instrument gives an average and each data point in the graph [Figure 4(b)] was the average of ten individual measurements. Most measured values occurred in the range from 0.14 to 0.16 V, and no particular trends in voltage change with time could be detected over the 2-week period of measurements. There was no consistent indication of any significant degradation of voltage over the 14-day period of sustained loading. Current was also measured with a Keithly precision digital ammeter; the measured values of current were 20.3 ± 10 nA.

Figure 5 shows a bolted composite specimen prior to and after application of sustained loading over 2 weeks. There are visual indications of copper deposition in the vicinity of the bolt. Microscopic observations of the bolted connection subjected to sustain loading (Figure 6) confirmed deposition of copper

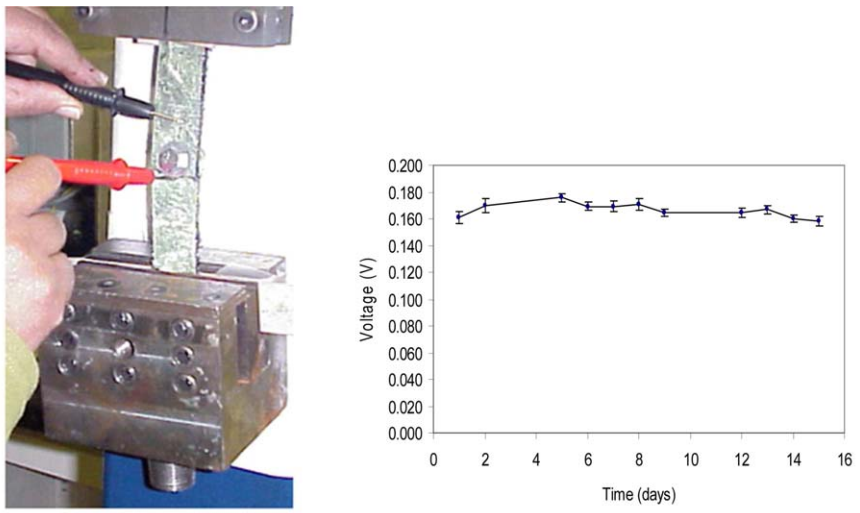

(a) Measurement condition (b) mean of potential difference versus time

Figure 4. Electric potential difference versus time under sustained service load: (a) measurement condition and (b) mean of potential difference versus time. [Color figure can be viewed in the online issue, which is available at wileyonlinelibrary.com.]

(a) Before sustained loading (b) After sustained loading application

Figure 5. Visual appearance of the bolted joint prior to and after sustained loading. [Color figure can be viewed in the online issue, which is available at wileyonlinelibrary.com.]

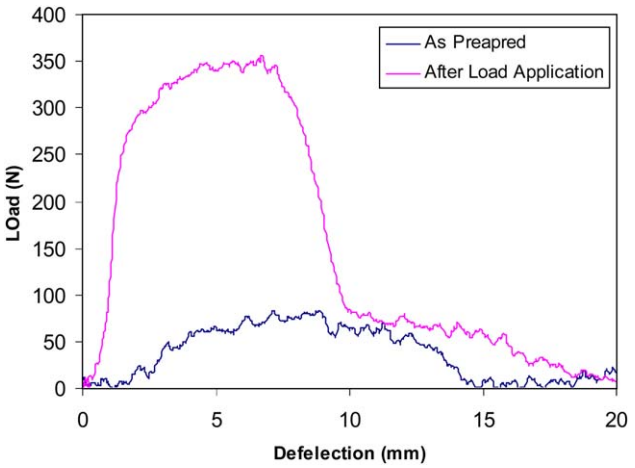

Figure 8. Load-deflection curves for the "as-prepared" bolted composite specimen versus that for the specimen subjected to sustained service load prior to tensile loading to failure. [Color figure can be viewed in the online issue, which is available at wileyonlinelibrary.com.]

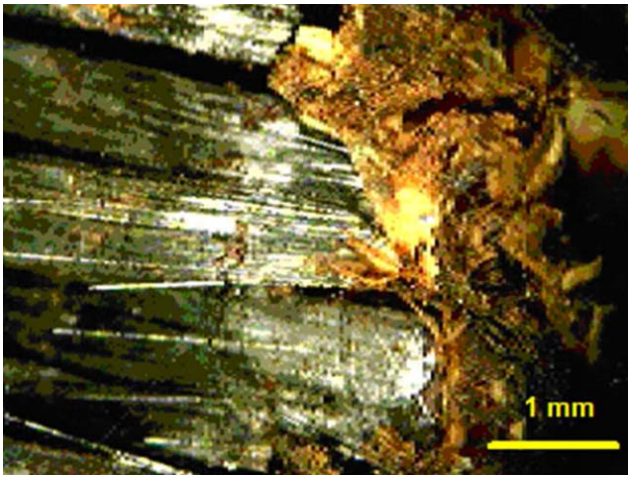

Figure 6. Microscopic image of the composite near bolt subjected to sustained loading. [Color figure can be viewed in the online issue, which is available at wileyonlinelibrary.com.]

within the highly stressed regions of the composite near the bolt. Scanning electron microscopic studies further confirmed these observations (Figure 7).

The experimental load-deflection curves shown in Figure 8 are for bolted composite specimens tested to failure prior to and after application of the sustained loading. Two specimens were tested after the same duration with (stressed) and without (nonstressed and control) stress application of sustained loading; the control specimen was not loaded whereas the other specimen was subjected to 14 days of sustained loading. The self-adaptive phenomenon in the (stressed) specimen subjected to sustained loading is observed to provide 4.5 times higher tensile load-carrying capacity when compared with the (nonstressed) control specimen (which was tested without application of sustained loading).

The specimens were 25-mm wide and 5-mm thick; the self-adapted and control specimens provided 350 N and 80 N load-carrying capacity, respectively, which translate into 0.64 and 2.8 MPa tensile stress, respectively. The sustained load of 35 N

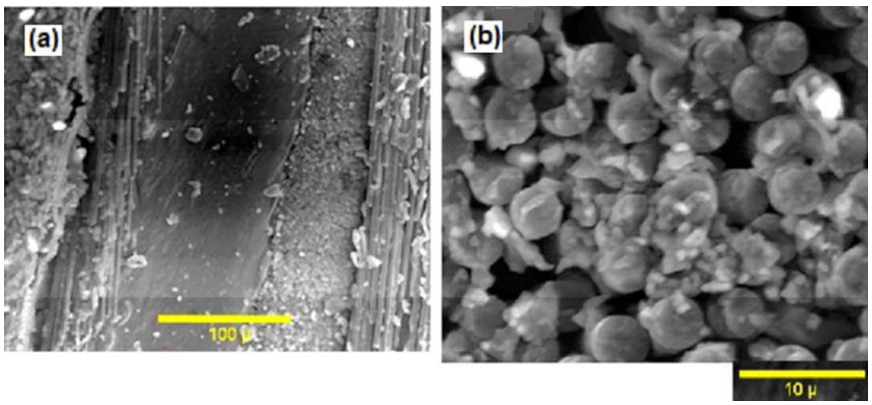

Figure 7. SEM microscopic images of cross-sections of composite near bolt subjected to sustained loading: (a) low magnification and (b) high magnification. [Color figure can be viewed in the online issue, which is available at wileyonlinelibrary.com.]

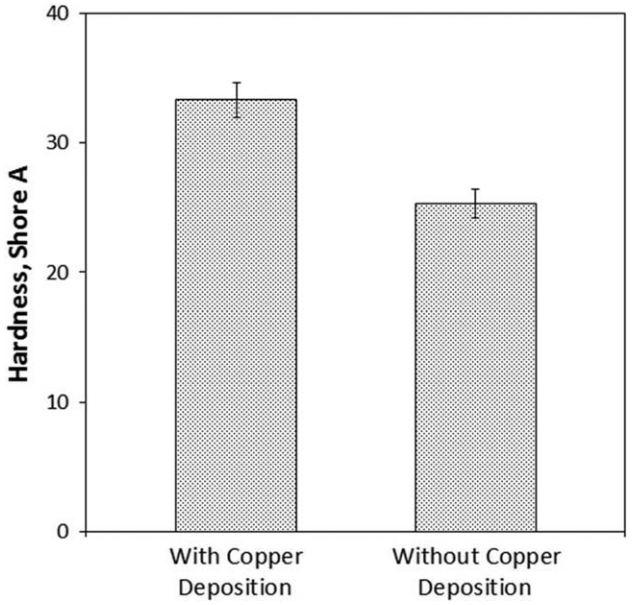

Figure 9. Mean values and standard error of the hardness test results for areas of polymer nanocomposite with and without copper deposition.

produced a service stress of 0.28 MPa in composite specimens. The self-adapted specimen also provided a high level of energy absorption capacity (measured as the area under the load-deflection curve) when compared with the control specimens. The mechanical test data complemented with the visual observations of failure modes indicated that the highly stressed area near the bolt was strengthened through self-adaptation (i.e., by copper deposition) under sustained loading. Failure was thus moved away from the critical area, which led to gains in strength and energy absorption capacity of the self-adapted joint.

The test data presented so far validated the occurrence of stress-induced redox reactions. It, however, remains to be verified that the deposits formed by redox reactions render mechanical strengthening effects. For this purpose, the areas of the solid electrolyte polymer nanocomposite near and away from bolt (with and without copper deposition) were subjected to hardness test; 10 tests were performed in each area. The deposits of stress-enabled redox reactions are observed in Figure 9 to increase the hardness of solid electrolyte polymer nanocomposite. This finding supports the mechanical reinforcement effect of the deposits formed by stress-enabled redox reactions.

Redox reactions were verified visually in above experiments. To further validate the self-adaptation principles, an attempt was made to confirm that the deposits formed by redox reactions are actually copper, and that zinc ionization occurs as the reduction step facilitating the oxidation of copper.

The self-adaptation effect essentially involves reduction of copper from the solid electrolyte solution [$Cu^{2+} + 2e^- \rightarrow Cu$ ($E = +0.34$ V)]. The self-adaptation effect requires a conductive surface in contact with the solid polymer electrolyte. Our experiments used a zinc-coated steel as the conductive surface in contact with the solid electrolyte. The self-adaptation effect is thus expected to involve dissolution of some zinc and iron within the solid polymer electrolyte [reverse of the reduction processes: $Zn^{2+} + 2e^- \rightarrow Zn$ ($E = -0.76$ V) and $Fe^{2+} + 2e^- \rightarrow Fe$ ($E = -0.44$ V)]. Energy dispersive X-ray spectroscopy (EDS) was undertaken to evaluate the nature of deposited matter which renders strengthening effects, and also to determine any chemical changes in the solid polymer electrolyte after the redox reaction.

The solid polymer electrolyte nanocomposite sheet was prepared as before, with the composition PVDF-HFP (29.8%), PC (17.6%), EC (34.7%), CuTf (17.8%), ZnO nanoparticles (0.05%), and Cu nanoparticles (0.03%). The sheet was sandwiched between a zinc-coated steel mesh (mesh size 40 × 36 #/cm^2, purchased from McMaster-Carr® Atlanta, GA) on one face and a silicon rubber (polysiloxane, good electrical insulator, McMaster-Carr® Atlanta, GA) on the opposite face. A grip was used to apply pressure upon the mesh supported on the active polymer nanocomposite sheet over a period of 48 h.

Figure 10 shows the visual appearance of the polymer nanocomposite sheet prior to and after contact with the zinc-coated steel mesh under pressure. Copper deposition was observed on

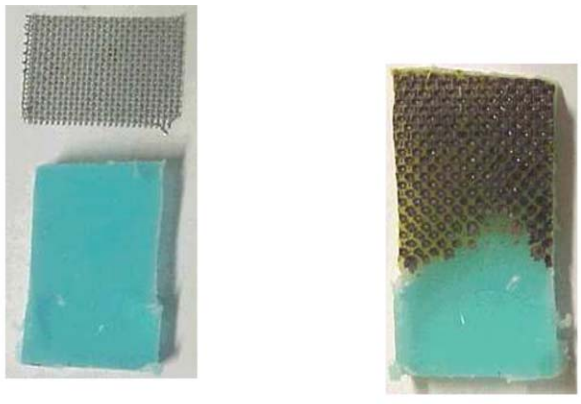

(a) Polymer sheet and the mesh prior to test (b) Polymer sheet after the test

Figure 10. Visual appearance of the solid electrolyte polymer nanocomposite sheet prior to and after the test: (a) polymer sheet and the mesh prior to test and (b) polymer sheet after the test. [Color figure can be viewed in the online issue, which is available at wileyonlinelibrary.com.]

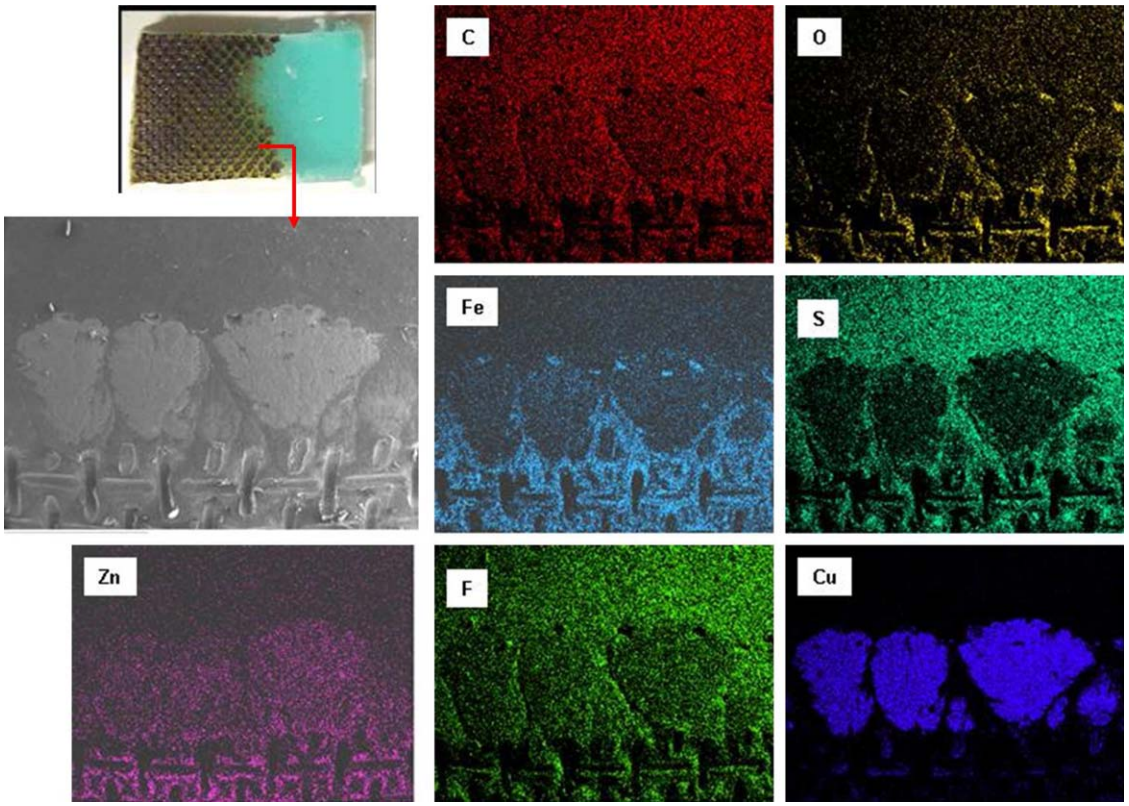

Figure 11. EDS maps of the active polymer nanocomposite sheet at the edges of the contacting metal mesh. [Color figure can be viewed in the online issue, which is available at wileyonlinelibrary.com.]

the polymer nanocomposite in areas contacting the metal mesh under pressure. Scanning electron microscope observations verified the metallic morphology of these areas which were in contact with metal mesh under pressure.

The EDS maps for the surface of solid electrolyte polymer nanocomposite sheet in contact with edges of the metal mesh under sustained pressure show indications of pronounced copper deposition in areas directly contacting the metal mesh under pressure (Figure 11). This probably results from transfer of copper from the less stressed regions just outside the area covered by the metal mesh. The area of the solid electrolyte polymer nanocomposite sheet which never contacted the mesh under sustained pressure exhibited uniform distribution of copper. EDS maps of the polymer nanocomposite surface after contact with zinc-coated steel mesh under sustained pressure (Figure 11) which directly contacted the metal mesh under pressure was darker in color indicating pronounced copper deposition. This confirms that the self-adaptation effect involves deposition of copper in the vicinity of the conductive surface under pressure. The open areas that did not directly contact the mesh had all elements evaluated (C, O, F, Fe, and Zn); the presence of Fe and Zn confirm the dissolution of zinc and iron within the solid polymer electrolyte during the self-adaptation process.

CONCLUSIONS

An inherently adaptive composite was developed, which in its preferred configuration, comprised PVDF-HFP solid polymer electrolyte embodying dissolved copper salt as well as copper and ZnO nanoparticles, interfaced with zinc metal. Elemental analyses were conducted using EDS techniques to validate the hypothesized stress-enabled redox reactions which render self-adaptation effects. The results confirmed that the deposits formed at and in the vicinity of conductive interfaces subjected to pressure were copper, with Zn and Fe present in neighboring areas. These observations confirm the reduction of copper cations and oxidation of zinc and iron in the stress-enabled redox process. Copper deposition was found to be more pronounced in the periphery of stressed conductive interface, which could result from transport of copper cations from outside the interface toward the interface, and their reduction/deposition at (and particularly at the periphery of) the interface. The face of the solid electrolyte polymer nanocomposite that was opposite to the stressed conductive interface exhibited (after redox reactions) a rise in Zn and Fe and a drop in Cu, which suggests transport of copper cations toward the stressed conductive interface, accompanied by the oxidation of zinc and iron followed by transport of their cations away from the conductive interface.

Bolted composite joints were used as example composite structures for verifying and demonstrating the self-adaptation phenomena. Laminated composites were processed using the solid electrolyte polymer nanocomposite matrix and woven carbon fiber reinforcement. The joints with steel bolts (including nuts and washers) exhibited a typical shear-out failure mode in single-lap shear tests. Under sustained (service) loads equivalent to 50% of the ultimate single-lap shear capacity, stress concentration at the conductive interface between the bolt and the

active polymer composite led to copper deposition at and in the vicinity of the bolt. The bolted joint subjected to sustained loading exhibited major gains in mechanical performance (strength) when compared with a similar unloaded joint. Hardness tests confirmed the local gain in mechanical performance associated with copper deposition in the vicinity of the bolt. Electric potentials and currents were detected between the critically stressed areas near the bolt and the less stressed areas away from the bolt; the electric potential did not degrade over an initial sustained loading period of 2 weeks. Longer-term tests indicated that the electric potential difference between the highly stressed and the less stressed areas of the bolted composite joint specimen eventually diminish after few weeks of sustained loading. Elemental (EDS) analyses confirmed the fundamental hypothesis which attributes the self-adaptation effects to the migration of copper cations toward and their deposition at stressed conductive interfaces. These analyses also provided further insight into the chemistry of the self-adaptation phenomena. These findings provide indications of the active period of self-adaptation for the specific structural systems and loading conditions considered here.

The self-adaptation phenomena were evaluated in this experimental program at early age. There is a need for longer-term evaluation of loaded as well as unloaded specimens to evaluate the system stability over time. Replicated tests are also needed to assess the statistical variations in the self-adaptation phenomena demonstrated in this investigation.

FUTURE WORK

The experimental work conducted in the research investigation provides proof-of-concept for self-adaptation phenomena occurring through stress-enabled redox reactions in the context of a solid polymer electrolyte. Detailed design of integrated system embodying all constituents in viable proportions for targeted structural applications, and processing and experimental verification of the integrated system would be a critical next step toward demonstrating and validating the new self-adaptation principle in application to specific composite structures.

ACKNOWLEDGMENTS

The research reported herein was supported by the US Army under Contract # W911W6-05-C-0010. The authors are thankful to Mr. Nate Bordick of the US Army for his guidance and support throughout the project.

REFERENCES

1. Kessler, M.; Sottos, N.; White, S. *Compos. Part A: Appl. Sci. Manuf.* **2003**, *34*, 743.
2. Ghosh, S. K. Self-healing Materials; Wiley-VCH: Weinheim, **2009**.
3. Kessler, M. Proc. Inst. Mech. Eng. Part G*: J. Aerosp. Eng.* **2007**, *221*, 479.
4. Baghdachi, J.; Perez, H.; Shah, A. In Smart Coatings III; Baghdachi, J.; Perez, H., Eds.; American Chemical Society: Washington, DC, **2010**, Chap. 1.
5. Hayes, S.; Jones, F.; Marshiya, K.; Zhang, W., *Comput. Part A: Appl. Sci. Manuf.* **2007**, *38*, 1116.
6. Kessler, M.; White, S. *Comput. Part A: Appl. Sci. Manuf.* **2001**, *32*, 683.
7. Barbero, E. J.; Ford, K. J. *J. Adv. Mater.* **2007**, *39*, 20.
8. Meyers, M. A.; Chen, P.-Y.; Lin, A. Y.-M.; Seki, Y. *Prog. Mater. Sci.* **2008**, *53*, 1.
9. Chen, P.-Y.; McKittrick, J.; Meyers, M. A. *Prog. Mater. Sci.* **2012**, *57*, 1492.
10. Currey, J. D. Bones: Structure and Mechanics; Princeton University Press: Princeton, NJ, **2002**.
11. Barthelat, F. *Philos. Trans. R. Soc. A: Math. Phys. Eng. Sci.* **2007**, *365*, 2907.
12. Soroushian, P.; Balachandra, A. M. *J. Intell. Mater. Syst. Struct.* **2013**, *24*, 441.
13. Fauci, A. S. Harrison's Principles of Internal Medicine; McGraw-Hill Medical: New York, **2008**.
14. White, S. R.; Sottos, N.; Geubelle, P.; Moore, J.; Kessler, M. R.; Sriram, S.; Brown, E.; Viswanathan, S. *Nature* **2001**, *409*, 794.
15. Patel, A. J.; Sottos, N. R.; Wetzel, E. D.; White, S. R. *Comput. Part A: Appl. Sci. Manuf.* **2010**, *41*, 360.
16. Varley, R. J.; Shen, S.; van der Zwaag, S. *Polymer* **2010**, *51*, 679.
17. Kalista, S. J.; Pflug, J. R.; Varley, R. *J. Polym. Chem.* **2013**, *4*, 4910.
18. Varley, R. In Self Healing Materials; Zwaag, S., Ed.; Springer: Netherlands, **2008**; Chap. 5.
19. Wu, D. Y.; Meure, S.; Solomon, D. *Prog. Polym. Sci.* **2008**, *33*, 479.
20. Varley, R. J.; van der Zwaag, S. *Polym. Int.* **2010**, *59*, 1031.
21. Hager, M. D.; Greil, P.; Leyens, C.; van der Zwaag, S.; Schubert, U. S. *Adv. Mater.* **2010**, *22*, 5424.
22. Richard, J. P.; O'Ferrall, R. M. *Adv. Phys. Org. Chem.* **2010**, *44*, xiii.
23. Díaz, D. D.; Kühbeck, D.; Koopmans, R. *J. Chem. Soc. Rev.* **2011**, *40*, 427.
24. Jang, H. B.; Rho, H. S.; Oh, J. S.; Nam, E. H.; Park, S. E.; Bae, H. Y.; Song, C. E. *Org. Biomol. Chem.* **2010**, *8*, 3918.
25. Jones, A. S.; Rule, J. D.; Moore, J. S.; White, S. R.; Sottos, N. R. *Chem. Mater.* **2006**, *18*, 1312.
26. Zwaag, S.; Schmets, A. J. M.; van der Zaken, G. Self Healing Materials: An Alternative Approach to 20 Centuries of Materials Science; Springer: Dordrecht, The Netherlands, **2007**.
27. Wouters, M.; Craenmehr, E.; Tempelaars, K.; Fischer, H.; Stroeks, N.; van Zanten, J. *Prog. Org. Coat.* **2009**, *64*, 156.
28. Liu, Y.-L.; Chen, Y.-W. *Macromol. Chem. Phys.* **2007**, *208*, 224.
29. Kelly, G. *Comput. Struct.* **2005**, *69*, 35.